Synthesis of Millimeter-Size Hexagon-Shaped Graphene Single Crystals on Resolidified Copper

Ali Mohsin,[†] Lei Liu,[†] Peizhi Liu,[‡] Wan Deng,[†] Ilia N. Ivanov,[§] Guoliang Li,[‡] Ondrej E. Dyck,[‡] Gerd Duscher,[‡,⊥] John R. Dunlap,[∥] Kai Xiao,[†,§] and Gong Gu[†,*]

[†]Department of Electrical Engineering and Computer Science and [‡]Department of Material Science and Engineering, The University of Tennessee, Knoxville, Tennessee 37996, United States, [§]Center for Nanophase Materials Sciences and [⊥]Materials Science and Technology, Oak Ridge National Laboratory, Oak Ridge, Tennessee 37831, United States, and [∥]Division of Biology, The University of Tennessee, Knoxville, Tennessee 37996, United States

ABSTRACT We present a facile method to grow millimeter-size, hexagon-shaped, monolayer, single-crystal graphene domains on commercial metal foils. After a brief *in situ* treatment, namely, melting and subsequent resolidification of copper at atmospheric pressure, a smooth surface is obtained, resulting in the low nucleation density necessary for the growth of large-size single-crystal graphene domains. Comparison with other pretreatment methods reveals the importance of copper surface morphology and the critical role of the melting−resolidification pretreatment. The effect of important growth process parameters is also studied to determine their roles in achieving low nucleation density. Insight into the growth mechanism has thus been gained. Raman spectroscopy and selected area electron diffraction confirm that the synthesized millimeter-size graphene domains are high-quality monolayer single crystals with zigzag edge terminations.

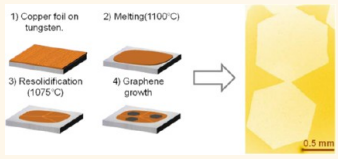

KEYWORDS: graphene · single crystal · millimeter size · melted and resolidified copper · CVD · nucleation and growth

Graphene, a strictly two-dimensional (2D) material, has received much attention since its exfoliation in 2004,[1] due to many unique physical properties originating from the honeycomb arrangement of carbon atoms.[2] In order to bring about practical applications of graphene, approaches toward its large-scale production have been actively explored.[3] To this end, chemical vapor deposition (CVD) on transition metal surfaces is among the promising methods.[4,5] Copper has become a popular catalytic substrate, due to its low carbon solubility at typical growth temperatures.[6] Low- or atmospheric-pressure CVD-grown graphene on copper is polycrystalline,[7] formed by the coalescence of domains.[5,8] The polycrystalline nature lowers the overall electrical performance of CVD graphene-based devices,[9] although certain types of grain boundaries are relatively benign to electrical transport.[10] Recently, synthesis of hexagon-shaped single-crystal graphene domains attracted considerable interest in the graphene CVD community.[9,11−15] The hexagonal crystallite shape is desirable due to the well-defined edge geometry (zigzag),[14] which is shown to have interesting electronic properties.[16] In the earlier reports, the size of hexagonal single-crystal graphene domains was limited to tens of micrometers.[9,11−15] Later reports revealed that smooth copper surface morphology plays an important role to limit the initial density of graphene nuclei in order to grow large single-crystal domains.[17−21] By extended thermal annealing of the Cu foil, Wang *et al.* demonstrated square-shaped submillimeter single-crystal graphene domains with jagged edges.[17] Yan *et al.* reported the synthesis of hexagonal single-crystal graphene domains up to 2.4 mm in size, but the growth required prolonged pretreatment of copper foils including high-pressure annealing (~2 atm) for extended period of time (7 h) following electrochemical polishing.[18] Li *et al.* synthesized ~1.8 mm, single-crystal graphene domains by reducing copper evaporation from the inner walls of a copper enclosure used as a catalytic substrate, but the synthesis required low pressure (~70 mTorr) for prolonged time (~6 h).[19] To overcome the barriers imposed by solid copper on the control of nucleation density, Geng *et al.* and Wu *et al.* grew graphene crystallites on liquid copper.[20,21] Contrary to intuition, graphene nucleation density was higher on

* Address correspondence to ggu1@utk.edu.

Received for review July 4, 2013 and accepted September 4, 2013.

Published online September 04, 2013
10.1021/nn4034019

liquid copper than in the aforementioned reports, and the domain size was limited to 200 μm.[20,21] The possible reason, subjected to further studies, is that the gradient in carbon concentration during cooling leads to convection within the liquid copper,[22] which limits the size of graphene domains. In general, a facile synthesis method, which does not require special setup (for high- or low-pressure growth) or prolonged, high-temperature substrate pretreatments but still achieves millimeter-size, single-crystal graphene domains with well-defined edge geometry, is highly desirable.

In this work, millimeter-size hexagon-shaped single-crystal monolayer graphene domains are synthesized by atmospheric-pressure CVD (APCVD) on commercial metal foils after brief *in situ* pretreatment. By first melting and then resolidifying copper on a tungsten foil, a relatively smooth surface is obtained, confirmed by atomic force microscopy (AFM). The smooth copper surface results in a low graphene nucleation density, which enables the growth of large-size domains. Growth temperature and hydrogen partial pressure also play very important roles in limiting the nucleation density. Formation of uniform, monolayer, single-crystal graphene domains with zigzag edges was confirmed by Raman spectra and area mapping as well as selected area electron diffraction (SAED).

RESULTS AND DISCUSSION

We chose APCVD as our synthesis technique due to its simple setup. Growth at atmospheric pressure also avoids copper evaporation from the foil substrate, an issue associated with low-pressure CVD (LPCVD).[23] Figure 1a summarizes our method. Commercial copper foils of 99.999% purity were used to minimize nucleation due to impurities.[12] After very brief initial cleaning (see Methods for details) to remove any manufacturer coating, copper foils were placed on a tungsten foil to prevent dewetting of liquid copper on quartz.[20,21] To melt the copper, the substrate was heated at 1100 °C for 30 min under argon (940 sccm) and hydrogen (60 sccm). Then, the temperature was slowly ramped down to 1075 °C, that is, below the melting point of bulk copper (1084 °C), and the copper resolidified. Growth was carried out at this temperature, with 0.1% dilute methane in argon, hydrogen, and argon flowing at 46, 100, and 854 sccm, respectively, for 5 h (see Supporting Information Figure S1 for complete process diagram). Figure 1b shows a photograph of the graphene domains, made visible by oxidizing the unprotected copper surface by heat treatment on a hot plate.[17] Figure 1c shows a scanning electron microscope (SEM) image of the two graphene domains, identified in Figure 1b. The side-to-side distance is ~1 mm, and the 120° angles between the hexagon sides are clearly identifiable. Compared to previous reports on millimeter-size single-crystal graphene,[18,19]

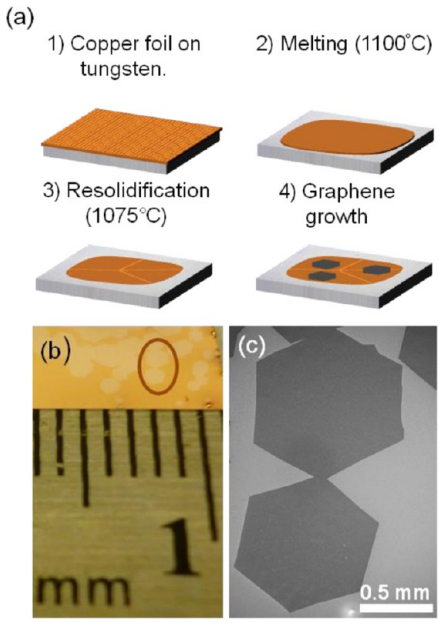

Figure 1. (a) Simple method to grow millimeter-size graphene single crystals on melted and resolidified copper. (b) Photograph of the synthesized domains. (c) SEM image of an area identified in (b).

domains obtained in this study are more regular hexagons without rough edges.

Graphene growth on copper initiates by the formation of small stable single-crystal clusters, which then coalesce to form a polycrystalline film.[5] Therefore, the key step in growing millimeter-size domains is to have only one single-crystal cluster in ~1 mm^2 area. To reveal the importance of copper surface morphology in achieving this goal, we compare in Figure 2 graphene grown on different copper surfaces for 30 min at the same temperature (1075 °C). Figure 2a shows nearly complete graphene coverage on a solid copper foil that was annealed at 1075 °C for 30 min before the graphene growth, with small uncovered copper surface areas as the one indicated by an arrow. Figure 2b shows the graphene grown on electro-polished foils (also annealed at 1075 °C for 30 min before the graphene growth), where the fraction of uncovered copper regions is much higher compared to that in Figure 1a, indicating lower nucleation density on electro-polished foils. However, the nucleation density is still too high for the growth of millimeter-size domains. In Figure 2c, on melted and resolidified copper, only three hexagonal nuclei are present in a ~3 mm^2 area.

Figure 2d shows a higher magnification image of the boxed region in Figure 2a. Areas of darker contrasts, indicated by arrows, are assigned as multilayer graphene.[6] To further clarify the growth on thermally annealed solid copper, we show in Figure S2 SEM images of graphene crystallites grown over a shorter duration of 10 min at the same temperature of 1075 °C. Figure S2a shows that a high density of graphene nuclei roughly follows the underlying rolling features

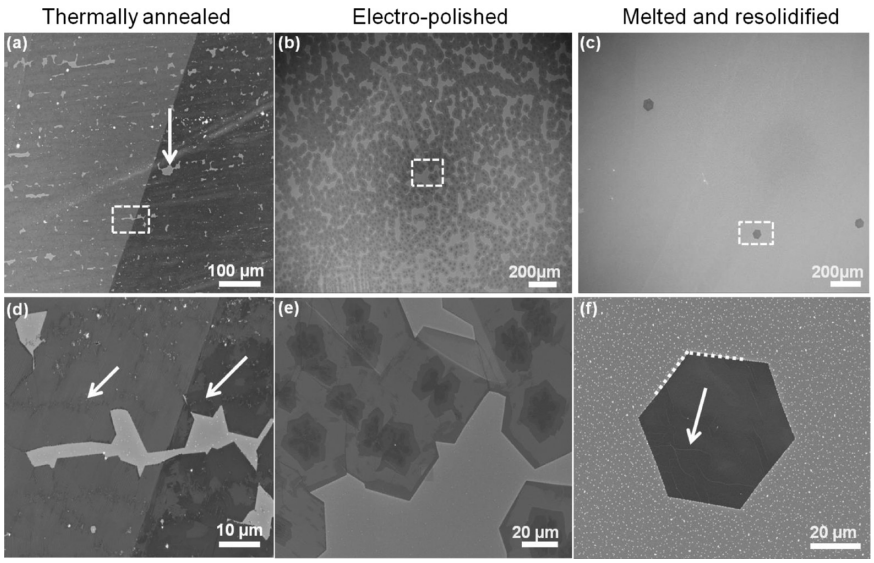

Figure 2. Comparison of graphene nucleation density on different copper surfaces. SEM images of (a) thermally annealed solid copper; (b) electro-polished foil; (c) melted and resolidified copper. (d–f) Higher magnification images of the areas identified in (a–c).

present on commercial copper foils,[12,17,18] while Figure S2b,c indicates that graphene nucleation density is low in the regions between the rolling marks. When the growth was carried out for 30 min, however, the dense graphene nuclei on the thermally annealed foil coalesced to result in nearly complete graphene coverage. The higher initial nucleus density on the rolling features also leads to the formation of small multilayer graphene regions.

Figure 2e is a higher magnification image of the boxed region in 2b. Interestingly, all the graphene domains have small multilayer regions at the centers. This is due to the mounds introduced during electropolishing, as will be shown later, which can have higher density of active carbon species, leading to stable graphene clusters.[24] The domain size in this case is ~40 μm.

Figure 2f is a higher magnification image of the region boxed in 2c, showing a graphene domain on melted and resolidified copper, which exhibits a distinct hexagon shape with sides 120° apart, as well as a uniform contrast within it, indicating the absence of multilayer regions. The domain size in this case is ~55 μm, larger than obtained on electro-polished foils. The wrinkle-like features can also be seen as indicated by an arrow. These are due to the rolling features on the tungsten foil underlying the Cu foil, as will be shown later.

To understand the significant reduction in the graphene nucleation density on melted and resolidified copper as compared to thermally annealed and electro-polished foils, we show in Figure 3 the AFM topographical images of these copper foil surfaces. Figure 3a shows that the as-received copper foil surface is very irregular with a root-mean-square (rms) roughness of ~166 nm. Thermal annealing without melting and resolidification, as well as electro-polishing, reduces surface irregularities as shown by the line profiles in Figure 3e.

Noticeably, for the melted and resolidified copper, the surface roughness is only 8 nm and the surface profile is the smoothest in Figure 3e. Interestingly, in Figure 3d, an additional set of features can also be seen. These are due to the surface morphology of the underlying tungsten foil. To verify, we show in Figure S3a,c AFM images for the as-received tungsten foil as well as a foil annealed in the same manner as melting and resolidifying copper foils. The improvement in the surface roughness is slight, if any, after annealing (6.78 nm) compared to the as-received (6.96 nm), which is expected as tungsten is a refractory metal and the temperature at which we melt copper (1100 °C) is well below the melting point of tungsten (above 3000 °C). Nevertheless, the surface roughness of the tungsten foil (~7 nm) is low compared to as-received, electro-polished, and thermally annealed copper foils. As the resolidified copper surface largely conforms to the underlying W foil surface, the smooth Cu surface morphology originating from the smooth W surface is critical to the low nucleation density in graphene growth.

To complement the topographic information displayed by AFM images, we show in Figure S4 the SEM images at a tilt angle of 75° for the different copper surfaces discussed above. Figure S4a shows the rough topography of the as-received copper foil with rolling marks. The annealed solid copper surface in Figure S4b is smoother but still with significant rolling features. Figure S4c shows that mounds are introduced on the copper surface during electrochemical

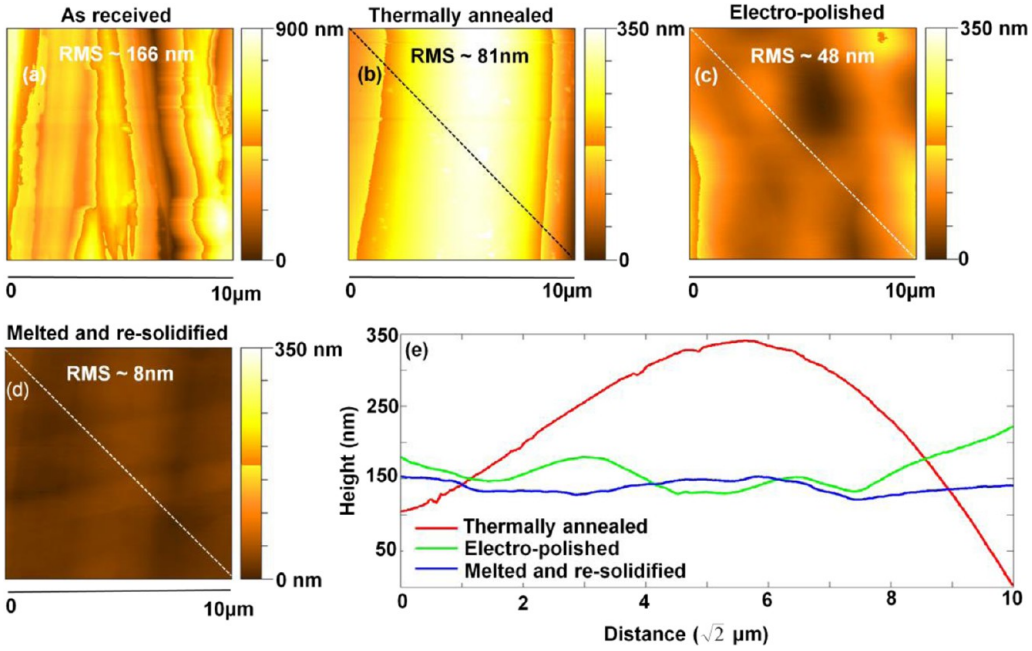

Figure 3. AFM topographical images of various copper surfaces. (a) As-received, (b) thermally annealed, (c) electro-polished, and (d) melted and resolidified. (e) AFM line profiles corresponding to the white dashed lines marked in (a−d).

polishing. Electro-polishing planarizes the Cu surface better than thermal annealing of solid copper but cannot completely eliminate rolling marks. The left-over rolling marks and the mounds introduced during polishing contribute to a nucleation density that is still high. Figure S4d shows the melted and resolidified copper, where visible features originate from the underlying W foil. The surface morphologies of as-received and annealed tungsten foils are shown by the SEM images in Figure S3, along with AFM images.

The above results show that the Cu surface morphology is one of the most important factors to limit graphene nucleation density. This can be understood from the thermodynamics and kinetics of the growth process. Since precursor adsorption is favorable on surface irregularities,[25] the local concentration of active carbon species, which lead to graphene growth, is higher along the rolling marks than in smooth regions. This higher concentration can overcome the thermodynamic barrier for nucleation,[25] leading to a high density of graphene nuclei. Moreover, diffusion of active carbon species is limited in the presence of rolling marks,[24,26] leading to the formation of multilayer graphene. In contrast, smooth copper surface morphology facilitates surface diffusion,[26] resulting in a lower nucleation density on melted and resolidified copper.

To highlight the importance of the melting−resolidification treatment as opposed to merely high-temperature annealing of solid copper, next we compare graphene domains obtained on copper foils annealed at 1080 °C (Figure 4a) and those melted at 1100 °C followed by resolidification (Figure 4b).

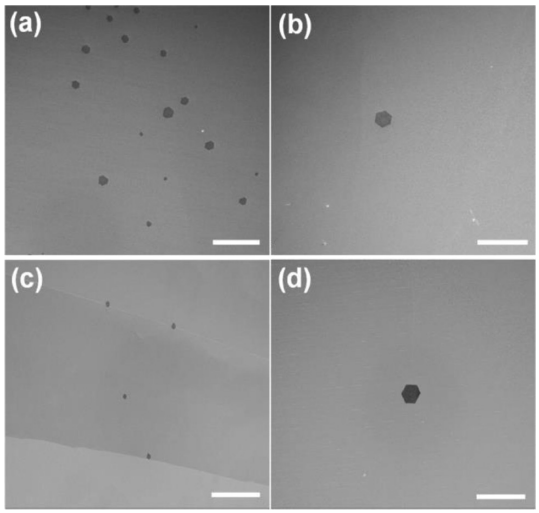

Figure 4. Dependence of graphene nucleation density on thermal pretreatment and growth temperature. (a,b) SEM images of graphene on copper foil annealed/melted for 30 min at (a) 1080 °C and (b) 1100 °C. Growth temperature (1075 °C) and growth time (30 min) were kept constant. (c,d) SEM images of the graphene grown at (c) 1050 °C and (d) 1075 °C. Melting temperature (1100 °C) and growth time (30 min) were fixed. Scale bars are 0.2 mm.

To reduce the defects introduced during the resolidification, the temperature ramp down rate was fixed at 1 °C/min in this study. In both cases, graphene growth was carried out at 1075 °C for 30 min. Figure 4a,b indicates that graphene nucleus density/size is higher/smaller for the copper melted at 1080 °C compared to 1100 °C. At 1080 °C, a temperature very close to but below the melting point of bulk copper (1084 °C), the copper surface is flowing. This movement removed the

majority of the rolling marks but did not eliminate their effect completely. Therefore, the surface is not sufficiently smooth, leading to the still high nucleation density. In contrast, only one large-size hexagonal graphene domain is present in ~1 mm^2 area on the copper that was melted at 1100 °C followed by resolidification.

Next we show the effect of growth temperature on nucleation density and grain size on resolidified Cu, with growth time fixed at 30 min. Figure 4c shows four graphene nuclei, each ~25 μm in size, in a ~1 mm^2 area, typical of the graphene grown at 1050 °C on resolidified copper. As the growth temperature increases to 1075 °C, only one ~65 μm graphene domain is present in ~1 mm^2. This temperature dependence can be explained in the framework of existing graphene nucleation model:[24] At the higher temperature, increased desorption rate and capture rate prevent further nucleation after the initial stage, while the increased capture rate due to higher carbon species' mobility increases growth rate and therefore the grain size grown in a fixed duration. Notice that the partition between the capture- and desorption-controlled regimes in the nucleation density−temperature dependence is very different in APCVD than in LPCAVD studied in previous work.[24]

Hydrogen also plays an important role in graphene synthesis.[5] Vlassiouk *et al.* showed that hydrogen acts as both an activator and an etching reagent during graphene growth.[12] Although the presence of oxygen impurity in commonly used ultra-high-purity (UHP)-grade hydrogen is shown to be necessary for graphene etching,[27] our discussion below is independent of the exact chemistry as the O_2 impurity is inevitable unless a hydrogen purifier is incorporated in the CVD system. To gain further insight into the role of hydrogen in our experiments, we vary the hydrogen partial pressure during growth, while keeping synthesis temperature (1075 °C), dilute methane flow rate (46 sccm), total flow rate (1000 sccm), and growth time (90 min) constant. For three experiments, the hydrogen flow rate is 100 sccm during the first 60 min of growth followed by 30 min of growth with hydrogen flow rates of 80 sccm (Figure 5a), 90 sccm (Figure 5b), and 100 sccm (Figure 5c).

Comparison of Figure 5a−c seems to suggest that it is desirable to accelerate growth after initial nucleation by decreasing hydrogen partial pressure, but careful examination of Figure 5b indicates that secondary graphene domains begin to nucleate when hydrogen flow rate was decreased to 90 sccm and that the size of secondary graphene domains is significantly bigger in Figure 5a, where the hydrogen flow rate was reduced even further to 80 sccm. Hydrogen acts as an etching reagent and thus suppresses secondary nucleation. There is a competition between the growth of existing graphene domains and the formation of secondary

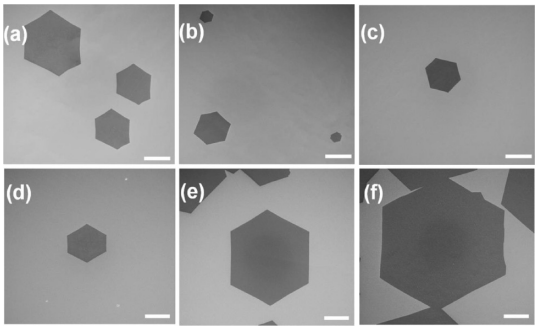

Figure 5. Dependence of nucleation density on hydrogen partial pressure and the increase in domain size with growth time. (a−c) SEM images of the graphene crystallites synthesized for 90 min, under 100 sccm of hydrogen during the first 60 min of growth followed by 30 min of (a) 80, (b) 90, and (c) 100 sccm hydrogen flow. (d,e) Graphene domains grown for (d) 100, (e) 200, and (f) 300 min, with a constant hydrogen flow rate (100 sccm). Scale bars are 0.2 mm.

nuclei. When the hydrogen flow rate is reduced, the local concentration of active carbon species is high enough that it can overcome the thermodynamic barrier for nucleation,[25] leading to secondary graphene domains. Also, when the hydrogen flow rate is reduced to 80 sccm in Figure 5a, the edges of the primary graphene domain begin to show an increased inward curvature compared to the graphene domain obtained in Figure 5c. Due to the formation of secondary graphene nuclei nearby, the effective rate of attachment of carbon species to the primary graphene domain is reduced, resulting in an inward curvature. Notice that the above analysis is not contradictory to previous work,[24] where nucleation does not occur after the initial stage due to the competition from capture. Here, the nucleus density is sufficiently low; therefore, new nuclei can form, not affected by existing nuclei at distances much longer than the mean travel distance of active carbon species.

Next in Figures 5d,e, we show the growth of graphene domains with time toward millimeter sizes. Synthesis temperature (1075 °C), dilute methane flow rate (46 sccm), and hydrogen flow rate (100 sccm) were all kept constant. For growth times of 100 min (Figure 5d), 200 min (Figure 5e), and 300 min (Figure 5f), the side-to-side distances for the graphene domains are ~0.3, ~0.63, and ~1 mm, respectively. This largely linear time dependence indicates that the growth velocity of the edge is constant as can be deduced as follows. The increase in the size of an existing domain is due to the attachment of carbon atoms to the growth front.[14,24] Due to the very low nucleus density, there is virtually no competition between nuclei in capturing the active carbon species. Therefore, the increase in a linear dimension of a growing crystallite is simply proportional to the diffusion rate (*i.e.*, average speed) of the active carbon species (see Supporting Information for more detailed analysis), which is constant at a fixed temperature.

Raman spectroscopy is an important graphene characterization technique to determine the number of

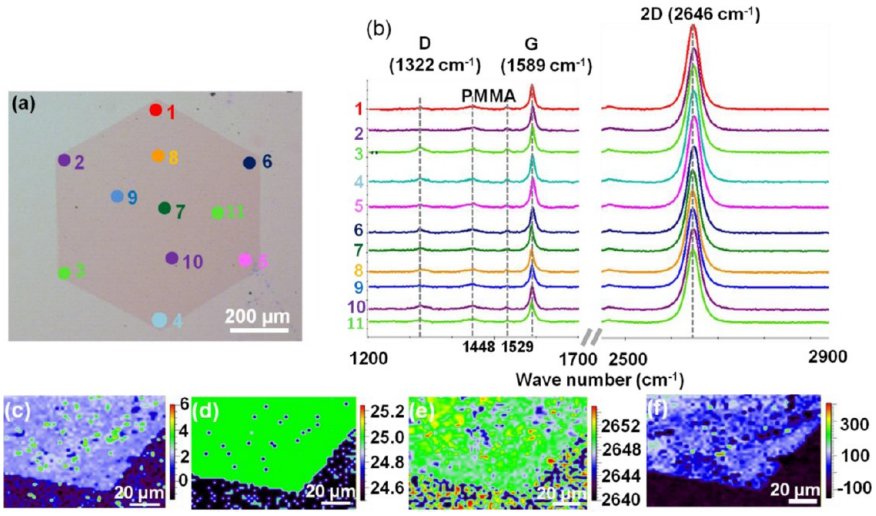

Figure 6. Raman characterization. (a) Optical image of the graphene crystallite transferred to a 300 nm SiO_2/Si substrate, (b) color-coded stacked Raman spectra corresponding to the spots identified in (a), (c) 2D to G peak intensity ratio (I_{2D}/I_G), (d) fwhm of the 2D peak, (e) position of the 2D peak, and (f) G to D peak intensity ratio (I_G/I_D) maps of another crystallite.

layers, the presence of defects,[28] as well as edge types.[29] Figure 6a shows an optical image of a graphene domain transferred to a 300 nm SiO_2/Si substrate. The color-coded stacked Raman spectra corresponding to the discrete points identified in Figure 6a are shown in Figure 6b. The important peaks, D (~1322 cm^{-1}), G (~1589 cm^{-1}), and 2D (~2646 cm^{-1}), agree well with the literarure.[30,31] The excellent consistency of these spectra indicates the uniformity of our synthesized domains. The 2D to G peak intensity ratio ($I_{2D}/I_G > 2$), the position of 2D peak (~2646 cm^{-1}), and the full width at half-maximum (fwhm) of the 2D peak (~33 cm^{-1}) suggest that the graphene crystallite is monolayer.[32,33] The high G to D peak intensity ratio (I_G/I_D) above ~10 at all spots including spots 3 and 4 at corners indicates high quality as well as zigzag edge termination of the graphene domain.[29] Two very weak peaks at 1448 and 1529 cm^{-1} are due to polymethyl methacrylate (PMMA) residue introduced during the transfer step;[34] their absolute intensities are very small compared to the G peak. To further reveal the spatial uniformity of the transferred graphene, the mappings of I_{2D}/I_G, fwhm and position of the 2D peak, and I_G/I_D are shown in Figure 6c–f. The mean values of 2D the peak position (~2650 cm^{-1}), I_{2D}/I_G ratio (>2), and 2D peak fwhm (~25 cm^{-1}) indicate that the synthesized domain is uniformly monolayer.[32,33] High average G to D peak intensity ratio (~100), along with its uniformity throughout the crystallite, indicates that the zigzag edges are of same high quality as the center of the graphene domain.

To demonstrate the single-crystal, monolayer structure of our synthesized graphene crystallites, we next show SAED results. An SEM image of a graphene domain transferred onto a transmission electron microscope (TEM) grid is shown in Figure 7a, where the edges of the graphene domain are identified by dashed lines. We took SAED patterns in random TEM grid windows covered by the large graphene domain, including those near the edges and near the center of the graphene domain. Eight representative patterns are shown in Figure 7b–i. Hexagonal diffraction spots confirm the presence of graphene.[17–21] We define an angle θ, as shown in Figure 7b, to quantify the rotation of the graphene lattice at each location. The less than 3° maximum variation shows the single-crystal nature of the graphene domain.[21] To further confirm the monolayer nature of the graphene domain, we took SAED patterns at one location at different tilt angles from 0 to 30° (Figure S5). The plots of the intensity of first- and second-order spots (Figure S5h) decrease monotonically with the tilt angle, as expected for monolayer graphene.[21]

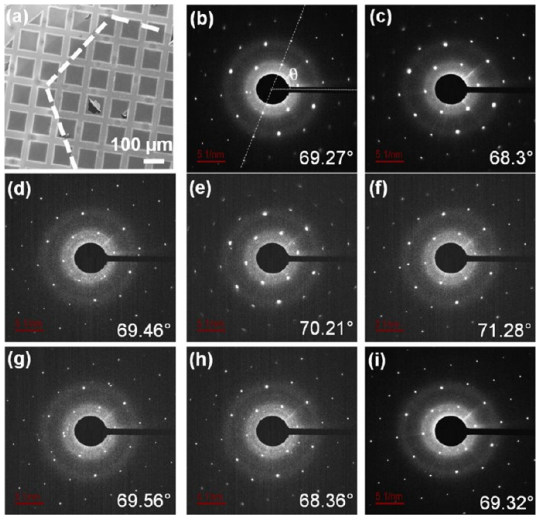

Figure 7. SAED characterization. (a) SEM image of the graphene domain transferred onto a TEM grid. The edges of the domain are delineated by dashed lines. (b–i) SAED patterns taken in different windows of the TEM grid.

Besides morphology improvement, we have investigated the crystallography changes of the resolidified Cu (see Figure S7). The surface of the resolidified Cu supported by the W foil is (111)-dominated, different from the (100)-dominated surface of the original cold-rolled Cu foil.[35] The grain size is many millimeters; therefore, grain boundaries are rarer than other possible nucleation sites. Moreover, we did not observe high densities of nuclei along any lines. We therefore conclude that the impact of grain boundaries in the resolidified Cu on the graphene domain size is at most minor. The influence of the new Cu grain orientation on other aspects of graphene growth will be further investigated in future work.

CONCLUSION

We have shown the growth of millimeter-size, single-crystal, monolayer graphene domains on commercial metal foils by a simple method that only requires brief *in situ* treatment of the substrate at atmospheric pressure. The nucleation density, a key factor in obtaining large-size single-crystal domains, strongly depends on the copper surface morphology. Thermal annealing below the copper melting point or electro-polishing cannot effectively eliminate surface irregularities; therefore, the nucleation density remains high after both treatments. When copper is melted and then resolidified on a tungsten foil, a smooth surface is obtained, resulting in a significant reduction in nucleation density. A relatively high growth temperature results in increased desorption of active carbon species, which further reduces the nucleation density. Hydrogen partial pressure is also critical since hydrogen suppresses secondary nucleation, which competes against existing nucleus growth and, therefore, skews the competition toward the latter. Raman spectroscopy indicates that the graphene domains obtained are single-layered with negligible defects and zigzag edge terminations. Moreover, SAED patterns confirm the single-crystal and monolayer natures of the synthesized domains.

METHODS

Graphene Synthesis. High-purity commercial copper foils (99.999%, 0.25 mm thick, Alfa-Aesar) and tungsten foils (99.95%, 0.05 mm thick, Alfa-Aesar) were used. The gases used in this research were of UHP-grade supplied by Airgas. Dilute methane (0.1%) balanced with argon was used as the carbon precursor. The growth was performed in a commercial CVD reactor (OTF-1200X-80-II-4CV-PE-SL, MTI) with a 2 in. diameter processing tube. Before growth, copper foils were dipped in dilute nitric acid and DI water for 20 s each and gently dried with a nitrogen gun. The copper foil was then placed on a tungsten foil and loaded into the quartz tube. The whole CVD system was then pumped down to the base pressure and then backfilled with argon and hydrogen. This procedure was repeated twice to minimize air residue in the subsequent growth process. After bringing the processing tube to atmospheric pressure, hydrogen and argon flow rates were adjusted to 60 and 940 sccm, respectively. The temperature was first ramped up to 1000 °C in 50 min and then to 1100 °C in 10 min. The temperature was kept constant for 30 min and then slowly ramped down (1 °C/min) to 1075 °C. After temperature stabilization for 10 min, dilute methane was introduced at a flow rate of 46 sccm and hydrogen and argon flow rates were changed to 100 and 854 sccm, respectively. After the growth, the furnace was cooled without changing the gas flows. The sample was unloaded below 80 °C under argon and hydrogen flow. To make graphene domains visible, the substrate was heated at 300 °C on a hot plate for 2 min. For electro-polishing, the as-received copper foil was used as the cathode in a home-built electrochemical cell, while another piece of copper foil was used as the anode. *ortho*-Phosphoric acid (85%, Sigma-Aldrich) was used as an electro-polishing solution, and foils were polished at a DC voltage of 5 V for 30 min.

For Raman characterization, graphene was transferred onto 300 nm SiO_2/Si substrate using PMMA.[6] Immediately after spin-coating PMMA at 4000 rpm for 60 s, the substrate was then baked at 160 °C for 10 min on a hot plate. Tungsten was then etched away by a tungsten etchant (Tungsten etch TFW, Transene Company), and copper was removed by a copper etchant (APS-100, Transene Company). The membrane was then transferred onto a clean SiO_2/Si substrate, and PMMA was removed by subsequent dipping in acetone (~4 h) and choloform (overnight) at room temperature. For SAED characterization, a graphene/PMMA membrane was scooped onto a TEM grid (Quantifoil) directly. The PMMA was then removed by thermal annealing at 370 °C for 2 h in 100 sccm of hydrogen and 1000 sccm of argon.

Scanning electron microscope images were acquired using a LEO 1525 SEM operated at 5 kV. SAED patterns were obtained using a Zeiss Libra 200 MC TEM operated at 200 kV. Raman spectra were recorded using a Renishaw confocal Raman microscope with 633 nm laser excitation. Atomic force microscopy (Asylum, Oxford Instruments) was carried out in the tapping mode in air at room temperature.

Conflict of Interest: The authors declare no competing financial interest.

Acknowledgment. This work was partially supported by NSF (ECCS-1231808) and DARPA (approved for public release; distribution is unlimited). A portion of this research was conducted at the Center for Nanophase Materials Sciences, which is sponsored at Oak Ridge National Laboratory by the Scientific User Facilities Division, Office of Basic Energy Sciences, U.S. Department of Energy. The authors thank G. Jones for his help in SEM imaging.

Supporting Information Available: Detailed process diagram, graphene growth on thermally annealed solid copper at reduced time duration, AFM area map of as-received and annealed tungsten foil, tilted SEM images of various copper surfaces as well as tungsten foil, and SAED patterns at different tilt angles. This material is available free of charge *via* the Internet at http://pubs.acs.org.

REFERENCES AND NOTES

1. Novoselov, K. S.; Geim, A. K.; Morozov, S. V.; Jiang, D.; Zhang, Y.; Dubonos, S. V.; Grigorieva, I. V.; Firsov, A. A. Electric Field Effect in Atomically Thin Carbon Films. *Science* **2004**, *306*, 666–669.
2. Geim, A. K.; Novoselov, K. S. The Rise of Graphene. *Nat. Mater.* **2007**, *6*, 183–191.
3. Novoselov, K. S.; Fal'ko, V. I.; Colombo, L.; Gellert, P. R.; Schwab, M. G.; Kim, K. A Roadmap for Graphene. *Nature* **2012**, *490*, 192–200.
4. Bae, S.; Kim, H.; Lee, Y.; Xu, X.; Park, J.-S.; Zheng, Y.; Balakrishnan, J.; Lei, T.; Kim, H. R.; Song, Y. I.; *et al.* Roll-to-roll Production of 30-Inch Graphene Films for Transparent Electrodes. *Nat. Nanotechnol.* **2010**, *5*, 574–578.

5. Mattevi, C.; Kim, H.; Chhowalla, M. A Review of Chemical Vapour Deposition of Graphene on Copper. *J. Mater. Chem.* **2011**, *21*, 3324–3334.
6. Li, X.; Cai, W.; An, J.; Kim, S.; Nah, J.; Yang, D.; Piner, R.; Velamakanni, A.; Jung, I.; Tutuc, E.; *et al.* Large-Area Synthesis of High-Quality and Uniform Graphene Films on Copper Foils. *Science* **2009**, *324*, 1312–1314.
7. Huang, P. Y.; Ruiz-Vargas, C. S.; Zande, A. M.; van der Whitney, W. S.; Levendorf, M. P.; Kevek, J. W.; Garg, S.; Alden, J. S.; Hustedt, C. J.; Zhu, Y.; *et al.* Grains and Grain Boundaries in Single-Layer Graphene Atomic Patchwork Quilts. *Nature* **2011**, *469*, 389–392.
8. Li, X.; Cai, W.; Colombo, L.; Ruoff, R. S. Evolution of Graphene Growth on Ni and Cu by Carbon Isotope Labeling. *Nano Lett.* **2009**, *9*, 4268–4272.
9. Yu, Q.; Jauregui, L. A.; Wu, W.; Colby, R.; Tian, J.; Su, Z.; Cao, H.; Liu, Z.; Pandey, D.; Wei, D.; *et al.* Control and Characterization of Individual Grains and Grain Boundaries in Graphene Grown by Chemical Vapour Deposition. *Nat. Mater.* **2011**, *10*, 443–449.
10. Tsen, A. W.; Brown, L.; Levendorf, M. P.; Ghahari, F.; Huang, P. Y.; Havener, R. W.; Ruiz-Vargas, C. S.; Muller, D. A.; Kim, P.; Park, J. Tailoring Electrical Transport Across Grain Boundaries in Polycrystalline Graphene. *Science* **2012**, *336*, 1143–1146.
11. Robertson, A. W.; Warner, J. H. Hexagonal Single Crystal Domains of Few-Layer Graphene on Copper Foils. *Nano Lett.* **2011**, *11*, 1182–1189.
12. Vlassiouk, I.; Regmi, M.; Fulvio, P.; Dai, S.; Datskos, P.; Eres, G.; Smirnov, S. Role of Hydrogen in Chemical Vapor Deposition Growth of Large Single-Crystal Graphene. *ACS Nano* **2011**, *5*, 6069–6076.
13. Wu, B.; Geng, D.; Guo, Y.; Huang, L.; Xue, Y.; Zheng, J.; Chen, J.; Yu, G.; Liu, Y.; Jiang, L.; *et al.* Equiangular Hexagon-Shape-Controlled Synthesis of Graphene on Copper Surface. *Adv. Mater.* **2011**, *23*, 3522–3525.
14. Luo, Z.; Kim, S.; Kawamoto, N.; Rappe, A. M.; Johnson, A. T. C. Growth Mechanism of Hexagonal-Shape Graphene Flakes with Zigzag Edges. *ACS Nano* **2011**, *5*, 9154–9160.
15. Wu, W.; Jauregui, L. A.; Su, Z.; Liu, Z.; Bao, J.; Chen, Y. P.; Yu, Q. Growth of Single Crystal Graphene Arrays by Locally Controlling Nucleation on Polycrystalline Cu Using Chemical Vapor Deposition. *Adv. Mater.* **2011**, *23*, 4898–4903.
16. Tian, J.; Cao, H.; Wu, W.; Yu, Q.; Chen, Y. P. Direct Imaging of Graphene Edges: Atomic Structure and Electronic Scattering. *Nano Lett.* **2011**, *11*, 3663–3668.
17. Wang, H.; Wang, G.; Bao, P.; Yang, S.; Zhu, W.; Xie, X.; Zhang, W.-J. Controllable Synthesis of Submillimeter Single-Crystal Monolayer Graphene Domains on Copper Foils by Suppressing Nucleation. *J. Am. Chem. Soc.* **2012**, *134*, 3627–3630.
18. Yan, Z.; Lin, J.; Peng, Z.; Sun, Z.; Zhu, Y.; Li, L.; Xiang, C.; Samuel, E. L.; Kittrell, C.; Tour, J. M. Toward the Synthesis of Wafer-Scale Single-Crystal Graphene on Copper Foils. *ACS Nano* **2012**, *6*, 9110–9117.
19. Chen, S.; Ji, H.; Chou, H.; Li, Q.; Li, H.; Suk, J. W.; Piner, R.; Liao, L.; Cai, W.; Ruoff, R. S. Millimeter-Size Single-Crystal Graphene by Suppressing Evaporative Loss of Cu during Low Pressure Chemical Vapor Deposition. *Adv. Mater.* **2013**, *25*, 2062–2065.
20. Geng, D.; Wu, B.; Guo, Y.; Huang, L.; Xue, Y.; Chen, J.; Yu, G.; Jiang, L.; Hu, W.; Liu, Y. Uniform Hexagonal Graphene Flakes and Films Grown on Liquid Copper Surface. *Proc. Natl. Acad. Sci. U.S.A.* **2012**, *109*, 7992–7996.
21. Wu, Y. A.; Fan, Y.; Speller, S.; Creeth, G. L.; Sadowski, J. T.; He, K.; Robertson, A. W. Large Single Crystals of Graphene on Melted Copper Using Chemical Vapor Deposition. *ACS Nano* **2012**, *6*, 5010–5017.
22. Paronyan, T. M.; Pigos, E. M.; Chen, G.; Harutyunyan, A. R. Formation of Ripples in Graphene as a Result of Interfacial Instabilities. *ACS Nano* **2011**, *5*, 9619–9627.
23. Kidambi, P. R.; Ducati, C.; Dlubak, B.; Gardiner, D.; Weatherup, R. S.; Martin, M.-B.; Seneor, P.; Coles, H.; Hofmann, S. The Parameter Space of Graphene Chemical Vapor Deposition on Polycrystalline Cu. *J. Phys. Chem. C* **2012**, *116*, 22492–22501.
24. Kim, H.; Mattevi, C.; Calvo, M.; Oberg, J. Activation Energy Paths for Graphene Nucleation and Growth on Cu. *ACS Nano* **2012**, *6*, 3614–3623.
25. Ohring, M. *The Material Science of Thin Films*; Academic Press: New York, 1992.
26. Luo, Z.; Lu, Y.; Singer, D. W.; Berck, M. E.; Somers, L. A.; Goldsmith, B. R.; Johnson, A. T. C. Effect of Substrate Roughness and Feedstock Concentration on Growth of Wafer-Scale Graphene at Atmospheric Pressure. *Chem. Mater.* **2011**, *23*, 1441–1447.
27. Choubak, S.; Biron, M.; Levesque, P. L.; Martel, R.; Desjardins, P. No Graphene Etching in Purified Hydrogen. *J. Phys. Chem. Lett.* **2013**, *4*, 1100–1103.
28. Ferrari, A. C.; Meyer, J. C.; Scardaci, V.; Casiraghi, C.; Lazzeri, M.; Mauri, F.; Piscanec, S.; Jiang, D.; Novoselov, K. S.; Roth, S.; *et al.* Raman Spectrum of Graphene and Graphene Layers. *Phys. Rev. Lett.* **2006**, *97*, 187401.
29. Almeida, C. M.; Carozo, V.; Prioli, R.; Achete, C. A. Identification of Graphene Crystallographic Orientation by Atomic Force Microscopy. *J. Appl. Phys.* **2011**, *110*, 086101.
30. Vidano, R. B.; Fischbach, D. B. Observation of Raman Band Shifting with Excitation Wavelength for Carbons and Graphites. *Solid State Commun.* **1981**, *39*, 341–344.
31. Malard, L. M.; Pimenta, M. A.; Dresselhaus, G.; Dresselhaus, M. S. Raman Spectroscopy in Graphene. *Phys. Rep.* **2009**, *473*, 51–87.
32. Lenski, D. R.; Fuhrer, M. S. Raman and Optical Characterization of Multilayer Turbostratic Graphene Grown *via* Chemical Vapor Deposition. *J. Appl. Phys.* **2011**, *110*, 013720.
33. Lee, D. S.; Riedl, C.; Krauss, B.; von Klitzing, K.; Starke, U.; Smet, J. H. Raman Spectra of Epitaxial Graphene on SiC and of Epitaxial Graphene Transferred to SiO_2. *Nano Lett.* **2008**, *8*, 4320–4325.
34. Lin, Y.-C.; Jin, C.; Lee, J.-C.; Jen, S.-F.; Suenaga, K.; Chiu, P.-W. Clean Transfer of Graphene for Isolation and Suspension. *ACS Nano* **2011**, *5*, 2362–2368.
35. Wofford, J. M.; Nie, S.; McCarty, K. F.; Bartelt, N. C.; Dubon, O. D. Graphene Islands on Cu Foils: The Interplay between Shape, Orientation, and Defects. *Nano Lett.* **2010**, *10*, 4890–4896.